

Quantum Kinetic Rates within the Nonequilibrium Steady State

Loïc Joubert-Doriol,¹ Kenneth A. Jung,² Artur F. Izmaylov,² and Paul Brumer²

¹*Univ Gustave Eiffel, Univ Paris Est Creteil, CNRS, UMR 8208, MSME, F-77454 Marne-la-Vallée, France*

²*Chemical Physics Theory Group, Department of Chemistry, and Center for Quantum Information and Quantum Control, University of Toronto, Toronto, Ontario M5S 3H6, Canada*

(Dated: 5 September 2022)

The nonequilibrium steady state (NESS) of a quantum network is central to a host of physical and biological scenarios. Examples include natural processes such as vision and photosynthesis, as well as technical devices such as photocells, both activated by incoherent light (e.g. sunlight) and leading to quantum transport. Here, a completely general approach to defining components of a quantum network in the NESS, and obtaining rates of processes *between* these components is provided. Quantum effects are explicitly included throughout, both in (a) defining network components via projection operators, and (b) in determining the role of coherences in rate processes. As examples, the methodology is applied to model cases, two versions of the V-level system, and to the spin-boson model, wherein the role of the environment and of internal system properties in determining the rates is examined. In addition, the role of Markovian vs. non-Markovian contributions is quantified, exposing conditions under which NESS rates can be obtained by perturbing the nonequilibrium steady state.

I. INTRODUCTION

Quantum networks, i.e., collections of interacting states that are responsible for the transport of energy and matter, are ubiquitous in technology and in nature¹⁻⁴. Of particular importance are networks in the nonequilibrium steady state (NESS) driven for example by incident incoherent light (e.g. solar radiation). Examples include biophysically significant chemistry^{5,6} such as photosynthesis, or vision in molecular biology^{7,8} or photo and solar cells in device physics^{9,10}. In such processes, incoherent light is constantly being applied, the photoproduct continuously removed, and the initial state regenerated. The result is an NESS displaying (time independent) transport. Quantum NESSs are ubiquitous, but in need of further analysis and development.

The operation of the network, e.g., the rate at which the total network produces product, depends on the rates of transfer between components within the quantum network. Hence obtaining NESS rates between constituents that form the quantum network is a general, significant, challenge and of particular relevance to the natural operating conditions of thermal¹¹⁻¹⁴, biological¹⁵⁻²¹ and electronic²²⁻²⁵ systems that exhibit transport of matter and/or energy.

Efforts have been devoted to the study of such systems, but no systematic methodology for isolating and quantifying rates *within* the network has been developed. Similarly, there has been no versatile method proposed to define components of interest within the network. Studies thus far developed are tied to a particular choice of basis and particular network partitioning, a significant limitation that restricts their applicability. For example, our earlier NESS rate studies showed that the rate of producing product was determined by the long time scale associated with the absorption of the weak incoherent radiation.²⁶⁻²⁸ This limitation did correctly identify the rate determining step, but prevented obtaining rates of processes *within* the network. These issues are resolved in this paper, where we introduce a projection operator methodology that provides versatility in defining network “components”, and hence a methodology for isolating and extracting individual rates within the network.

We address these issues by beginning with the quantum Liouville equation that describes the evolution of the populations and coherences of a generic system. We introduce general projectors in the Liouville space that define the components of the network and cast the

Liouville dynamics into an equation of motion for the component populations by formally folding other characteristics such as the coherences into the population equations. This folding and consideration of the time-independent NESS limit results in a kinetic system of rate equations for arbitrarily defined network components.

The key focus on the NESS due to the significance noted above gives rates that are exact in the NESS case. The components comprising the resulting network are completely general, built upon the form of projection operators defining network partitioning. In particular, the methodology allows us to define partitions to extract rates *within* the network and to focus on various different processes and rates within the network.

This approach is relevant for arbitrary systems, and significantly generalizes previous works of quantum network analysis.^{1,20,21,29–31} We also provide insight into how and when one may measure these rates by explicitly perturbing the system out of its NESS and following the relaxation back to the steady state.

One additional note is in order. Natural light-induced processes are often experimentally studied via pulsed laser excitation, a light source that is totally alien to natural phenomena. For example, in the first steps in vision, retinal undergoes *cis* - *trans* isomerization, with the quantum yield of approximately 65%. Pulsed laser experiments imply that this process occurs on a timescale as fast as 60 femtoseconds³². However, this rate is of only marginal relevance for isomerization under natural incoherent light. Rather, what is required is *the rate of the process as it exists within the natural NESS*, a focus of this paper. Indeed, we show below that, as anticipated³³ the NESS rates are dramatically different from those obtained from a vertical excitation processes typical in ultrafast pulse excitations. This finding clearly demonstrates the need for theoretical/computational and experimental studies of the NESS regime to properly model natural processes.

This paper is organized as follows. Section II demonstrates how the Liouville equation, in the NESS limit, can be rewritten as a kinetic network, using Mori-Zwanzig and Feshbach projectors^{34–37}, allowing us to define a partitioning of the network into various constituents of interest. These projectors follow a set of basic rules, admit a wide range of possibilities and provide the formal definition of the NESS rate matrix. The approach is applied to two models in Sec. III based on a minimal model of energy transfer comprised of three-levels that is analytically soluble, and in Sec. IV to a non-equilibrium spin-boson model. The latter, a minimal model for processes that relate to isomerization in biophysics, uses a projector

defined in the nuclear space, which is beyond the treatment of previous methods.

Section V then deals with the issue of the validity of the rate expression away from the NESS, the relation to Markovian vs. non-Markovian dynamics, and the utility of perturbing the system away from the NESS to obtain the rate by a fitting procedure. We conclude with final remarks.

II. CONSTRUCTING KINETIC NETWORKS FROM THE LIOUVILLE EQUATION

A. The construction

Consider the Liouville equation

$$\dot{\hat{\rho}} = \mathcal{L}[\hat{\rho}], \quad (1)$$

where the system density matrix is $\hat{\rho}$, the dot denotes the time-derivative, and \mathcal{L} is the Liouvillian. The Liouvillians are designed to allow energy but not population flows between the system and the environment. Furthermore, since our goal is to construct the kinetic system of equations for a steady state, the Liouvillian is Markovian³⁸ and we assume that it has a single steady state, $\hat{\rho}_s$,

$$\mathcal{L}[\hat{\rho}_s] = 0. \quad (2)$$

For such Liouvillians, we propose to construct the general form of a kinetic network^{39,40}

$$\dot{\mathbf{p}} = \mathbf{k}\mathbf{p}, \quad (3)$$

where \mathbf{k} is a transition rate matrix, and \mathbf{p} is a vector of populations of interest. The corresponding steady state populations \mathbf{p}_s for N network components satisfy the global balance condition

$$\sum_{n \neq m}^N (k_{mn}p_{s,n} - k_{nm}p_{s,m}) = 0. \quad (4)$$

where $p_{s,n}$ is the n^{th} element of \mathbf{p}_s .

To define rates between arbitrary components, we divide the system into N components and consider the population flow between these parts. Populations of these parts can be defined as $p_n = \text{Tr}\{\hat{P}_n\hat{\rho}\}$ where $\{\hat{P}_n\}_{n=1}^N$ form a complete set of projectors in the Hilbert

space satisfying

$$\sum_n \hat{P}_n = 1, \quad (5)$$

$$\hat{P}_m \hat{P}_n = \hat{P}_n \delta_{mn}. \quad (6)$$

To partition the Liouville equation, the *Hilbert* space projectors \hat{P}_n are transformed into *Liouville* space projectors Π_n as

$$\Pi_n[\hat{B}] = \hat{\varrho}_n \text{Tr}\{\hat{P}_n \hat{B}\}, \quad (7)$$

where \hat{B} is any operator, and the operators $\{\hat{\varrho}_n\}_{n=1}^N$ are partitioned and renormalized components of the steady state density

$$\hat{\varrho}_n = \frac{\hat{P}_n \hat{\rho}_s \hat{P}_n}{\text{Tr}\{\hat{P}_n \hat{\rho}_s\}}. \quad (8)$$

The projectors $\{\Pi_n\}_{n=1}^N$ do not form a complete set, but can be completed with the addition of the projector \mathcal{Q} on the complementary Liouville space, with

$$\mathcal{Q} = 1 - \sum_{n=1}^N \Pi_n. \quad (9)$$

Applying the projectors $\{\Pi_n\}$ and \mathcal{Q} to Eq. (1) and using the relation $\text{Tr}\{\hat{P}_m \Pi_n[\hat{\rho}]\} = p_m$, gives the following set of equations involving the populations p_n :

$$\dot{p}_m = \sum_{n=1}^N \text{Tr}\{\hat{P}_m \mathcal{L}[\hat{\varrho}_n]\} p_n + \text{Tr}\{\hat{P}_m \mathcal{L} \mathcal{Q}[\hat{\rho}]\}, \quad (10)$$

$$\mathcal{Q}[\dot{\hat{\rho}}] = \sum_{n=1}^N \mathcal{Q} \mathcal{L}[\hat{\varrho}_n] p_n + \mathcal{Q} \mathcal{L} \mathcal{Q}[\hat{\rho}]. \quad (11)$$

Reduced dynamical equations containing only populations are obtained by integrating Eq. (11)

$$\begin{aligned} \mathcal{Q}[\hat{\rho}(t)] &= e^{\mathcal{Q} \mathcal{L} \mathcal{Q} t} \mathcal{Q}[\hat{\rho}(0)] \\ &+ \sum_{n=1}^N \int_0^t d\tau e^{\mathcal{Q} \mathcal{L} \mathcal{Q} (t-\tau)} \mathcal{Q} \mathcal{L}[\hat{\varrho}_n] p_n(\tau). \end{aligned} \quad (12)$$

and substituting the result into Eq. (10) to give

$$\begin{aligned} \dot{p}_m &= \sum_{n=1}^N \text{Tr}\{\hat{P}_m \mathcal{L}[\hat{\varrho}_n]\} p_n + \text{Tr}\{\hat{P}_m \mathcal{L} e^{\mathcal{Q} \mathcal{L} \mathcal{Q} t} \mathcal{Q}[\hat{\rho}(0)]\} \\ &+ \sum_{n=1}^N \int_0^t d\tau \text{Tr}\{\hat{P}_m \mathcal{L} e^{\mathcal{Q} \mathcal{L} \mathcal{Q} (t-\tau)} \mathcal{Q} \mathcal{L}[\hat{\varrho}_n]\} p_n(\tau). \end{aligned} \quad (13)$$

While Eq. (13) is exact, it is not yet in the form of Eq. (3). To arrive at the kinetic equation form, we focus on the steady state by substituting $\hat{\rho}(0)$ by $\hat{\rho}_s$ and \mathbf{p} by \mathbf{p}_s in Eq. (13). Then, \mathbf{p}_s becomes time-independent and the time integral can be done analytically. Furthermore, Eq. (11) for the steady state becomes $\mathcal{Q}[\hat{\rho}_s] = -\sum_{n=1}^N (\mathcal{Q}\mathcal{L}\mathcal{Q})^{-1} \mathcal{Q}\mathcal{L}[\hat{\rho}_n] p_{s,n}$, which brings Eq. (13) to the desired form

$$\dot{\mathbf{p}}_s = \mathbf{k}\mathbf{p}_s = \mathbf{0}, \quad (14)$$

where \mathbf{k} is a time-independent transition rate matrix whose elements are

$$k_{mn} = \text{Tr}\{\hat{P}_m(1 - \mathcal{L}(\mathcal{Q}\mathcal{L}\mathcal{Q})^{-1}\mathcal{Q})\mathcal{L}[\hat{\rho}_n]\}. \quad (15)$$

This rate definition satisfies global balance in the steady state (Eq. (4), i.e., $\mathbf{k}\mathbf{p}_s = \mathbf{0}$). Also, the construction of the rate matrix does not depend on the particular type of steady state, and can equally be applied to equilibrium or non-equilibrium circumstances.

The rates defined in Eq. (15) contain no approximations and are valid at the NESS. *They contain all information relevant to the transfer of population from one part to another, including the effects of the coherences.*

Note that the choice of the Hilbert space projectors used in Eq. (7) is not limited to any particular form, as long as they satisfy Eqs. (5-6). While we limit the presentation to cases where the projectors are defined either in the nuclear or electronic subspaces of the system, the projector form is flexible and can be chosen to suit any problem of interest.

Note that there is no need for dynamics simulations to obtain the steady state rates using Eq. (15). Rather, we can solve equation $\mathcal{L}\hat{\rho}_s = 0$ to obtain $\hat{\rho}_s$ and then construct the inverse of the superoperator $\mathcal{Q}\mathcal{L}\mathcal{Q}$. For small systems this is a simple task, which can be achieved by solving the system of Eqs. (10-11) in the steady state limit, as done in Appendix A. However, for large systems this is nontrivial, since the size of the Liouvillian scales quadratically with the basis size. Approaches that avoid explicit construction of the full Liouvillian, such as the stabilized conjugate gradient method⁴¹, or the iterative approach introduced in Ref. 27, are more efficient for large systems.

Finally, note that the resultant kinetic network Eq. (14) applies explicitly at the NESS. However, deviations from the steady state, and the associated return to the NESS are also of interest, as discussed in Sec. V, where non-Markovian and Markovian contributions to Eq. (13) from the complimentary space are analyzed in detail.

To examine rates in various systems of interest, and expose the utility of the choice of projectors, we consider two sample systems below.

III. V-SYSTEM

Consider first the V-system, a three level system that has been the subject of great interest in quantum optics⁴², coherence phenomena⁴³, population trapping⁴⁴ and qubit-qubit interactions and biophysical population dynamics⁴⁵, and as a minimal energy transfer donor-acceptor model²¹. In this case (Fig. 1) the Hamiltonian is of the form

$$\hat{H}_s = \epsilon_g |g\rangle\langle g| + \sum_{k=1}^2 \epsilon_k |k\rangle\langle k| + J(|1\rangle\langle 2| + |2\rangle\langle 1|) \quad (16)$$

The system contains a ground state $|g\rangle$ and two excited states $|1\rangle$ and $|2\rangle$ coupled with strength J . The system is connected to hot and cold baths. The hot bath excites the ground state to the excited states as

$$\mathcal{L}_H[\hat{\rho}] = 2 \sum_{k=1}^2 \Gamma_{H_k} \left(|1\rangle\langle g| \hat{\rho} |g\rangle\langle 1| - \frac{1}{2} [|g\rangle\langle g|, \hat{\rho}]_+ \right). \quad (17)$$

The cold bath is coupled with the system in two ways: (i) with a term that is responsible for de-excitation from the excited manifold back to the ground state

$$\mathcal{L}_C[\hat{\rho}] = 2 \sum_{k=1}^2 \Gamma_{C_k} \left(|g\rangle\langle k| \hat{\rho} |k\rangle\langle g| - \frac{1}{2} [|k\rangle\langle k|, \hat{\rho}]_+ \right), \quad (18)$$

and (ii) with terms responsible for relaxation and dephasing within the excited manifold

$$\begin{aligned} \mathcal{L}_D[\hat{\rho}] = & 2\Gamma_{D_f} \left(|2\rangle\langle 1| \hat{\rho} |1\rangle\langle 2| - \frac{1}{2} [|2\rangle\langle 2|, \hat{\rho}]_+ \right) \\ & + 2\Gamma_{D_b} \left(|1\rangle\langle 2| \hat{\rho} |2\rangle\langle 1| - \frac{1}{2} [|1\rangle\langle 1|, \hat{\rho}]_+ \right). \end{aligned} \quad (19)$$

Here $[|i\rangle\langle i|, \hat{\rho}]_+ = |i\rangle\langle i| \hat{\rho} + \hat{\rho} |i\rangle\langle i|$. The total master equation for the system reduced density matrix $\hat{\rho}$ is

$$\dot{\hat{\rho}} = -i[\hat{H}_s, \hat{\rho}] + \mathcal{L}_H[\hat{\rho}] + \mathcal{L}_C[\hat{\rho}] + \mathcal{L}_D[\hat{\rho}]. \quad (20)$$

To illustrate the versatility of our approach, we consider the V-system with two different choices of partitions, where ground and first excited states are either ungrouped (the standard case in the literature) or grouped together, while the second excited state always remains in its own group (Fig. 1). Unless stated otherwise, the numerical values of the parameters are set to the values in Table I.

TABLE I. Parameters employed in the V-system model in atomic units.

| ϵ_g | ϵ_1 | ϵ_2 | J | Γ_{H_1} | Γ_{C_1} | $\Gamma_{C_2}, \Gamma_{D_f}$ | $\Gamma_{H_2}, \Gamma_{D_b}$ |
|--------------|--------------|--------------|-------------------|---------------------|---------------------|------------------------------|------------------------------|
| 0 | 0.02 | 0.012 | $2 \cdot 10^{-5}$ | $1.5 \cdot 10^{-6}$ | $4.5 \cdot 10^{-6}$ | 10^{-9} | 0 |

A. Standard V-System

Using Eq. (20) and choosing the Hilbert space projectors $\{\hat{P}_i = |i\rangle\langle i|; i = g, 1, 2\}$ (in this case $\hat{\rho}_i = \hat{P}_i$) we obtain the equations of motion for the populations in the steady state as, where atomic units are used throughout,

$$\dot{\rho}_{gg} = -2(\Gamma_{H_1} + \Gamma_{H_2})\rho_{gg} + 2\Gamma_{C_1}\rho_{11} + 2\Gamma_{C_2}\rho_{22}, \quad (21)$$

$$\dot{\rho}_{11} = 2\Gamma_{H_1}\rho_{gg} - 2(\beta + \Gamma_{C_1} + \Gamma_{D_f})\rho_{11} + 2(\beta + \Gamma_{D_b})\rho_{22}, \quad (22)$$

$$\dot{\rho}_{22} = 2\Gamma_{H_2}\rho_{gg} + 2(\beta + \Gamma_{D_f})\rho_{11} - 2(\beta + \Gamma_{C_2} + \Gamma_{D_b})\rho_{22}, \quad (23)$$

and where we used the definitions

$$\beta = \frac{J^2\Gamma^*}{(\Gamma^*)^2 + \Delta^2}, \quad (24)$$

$$\Gamma^* = \Gamma_{C_1} + \Gamma_{C_2} + \Gamma_{D_f} + \Gamma_{D_b}, \quad (25)$$

$$\Delta = \epsilon_2 - \epsilon_1. \quad (26)$$

Here, β represents the component of the rate induced by the coherence. Further details regarding the derivation of these equations are provided in Appendix B.

Given Eqs. (21) - (23) the rates between state 1 and state 2 are seen to be

$$k_{21} = 2(\beta + \Gamma_{D_f}), \quad (27)$$

$$k_{12} = 2(\beta + \Gamma_{D_b}). \quad (28)$$

The forward rate k_{21} drives the population from ρ_{11} to ρ_{22} , while the backward rate k_{12} transfers the population in the reverse direction. Both rates contain two terms originating from distinct mechanisms: (1) The term β quantifies population transfer through the coherences ρ_{12} . Its presence is a direct result of rewriting the equations of motion of the system entirely in terms of populations, i.e., from making the populations implicitly dependent on the coherences. (2) The terms $2\Gamma_{D_f}$ or $2\Gamma_{D_b}$ give population transfer through the phonon bath. Note that if one regards the coherences as quantum, then the first term is a quantum

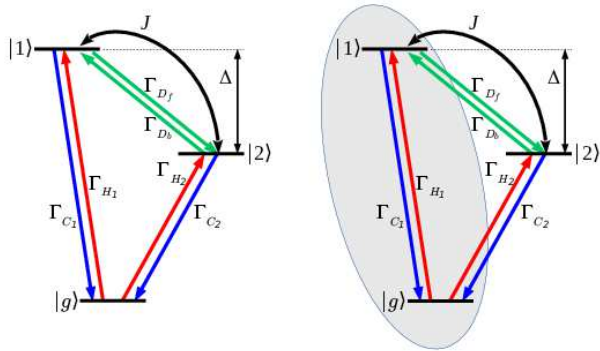


FIG. 1. Left: Depiction of the V-system. The hot bath transition is in red, cold bath transition are in blue, and the dephasing bath is in green. Δ denotes the excited state splitting. Right: The grouped V-system. The states enclosed in light blue depict the composite state A , which is comprised of the ground state and the first excited state.

contribution and the second is classical. Interestingly, both k_{12} and k_{21} show the same dependence on β ; that is, they only differ through the effect of the coupling to the bath. Hence the coherence term does not favor the forward or backward rate, nor does the sign of the level spacing Δ , since it enters as Δ^2 . Rather, it is the coupling to the bath that determines the directionality of the population flow.

Note that defining the projectors as $\{\hat{P}_i = |i\rangle\langle i|; i = g, 1, 2\}$ has successfully isolated the specific rate between states 1 and 2; indirect rates of population transfer between states 1 and 2, such as via $\Gamma_{C1} + \Gamma_{H2}$, do not participate.

Although the V-system is a simple model, examining the parameter dependence of the system and bath couplings is warranted to suggest dependences in large natural systems. When the bath-induced coupling between state $|1\rangle$ and $|2\rangle$ is zero, i.e., $\Gamma_{Df} = \Gamma_{Db} = 0$, the larger the Γ^* or Δ , the smaller the $k_{12} = k_{21}$ rate. For degenerate states, $\Delta = 0$, the transfer rate decreases as Γ^* increases, due to destructive effects of the bath on the coherences. When $J = 0$ population transfer is through \mathcal{L}_D , and the rate of excited state transfer resembles a classical rate^{46,47} in which the transfer is mediated through the bath instead of via the coherences between the excited states. Limiting cases such as those described above demonstrate that our rate definition agrees with previous analysis of quantum networks and the role that coherences play in them.^{15,21,29–31,48,49}

Additional parameters of interest include those that induce asymmetry²¹. As noted above, the nondegenerate case where $\Delta \neq 0$ [from Eqs. (22) and (23)], is detrimental to the rate.

Asymmetry can also be introduced by having different parameters for the two excited states. For example, we can design a “circular” flow by making $\Gamma_{D_f} \gg \Gamma_{D_b}$, and $\Gamma_{H_1} \gg \Gamma_{H_2}$ so that (i) the channel using $\Gamma_{H_1}/\Gamma_{C_1}$ pumps population from ground to first excited state; (ii) the channel using $\Gamma_{D_f}/\Gamma_{D_b}$ transfers population from the first state to the second excited state; and (iii) the population is dumped from the second excited state to the ground state using the $\Gamma_{H_2}/\Gamma_{C_2}$ channel. Hence, increasing Γ_{D_f} and Γ_{C_2} accelerates the population decay from state 1 to the ground state through state 2.

Further details regarding the interdependence of β on Δ and the bath parameters is provided in Fig. 2. The value of β is seen to behave monotonically at lower $\Gamma = \Gamma_{C_2} = \Gamma_{D_f}$ values, with larger Δ leading to smaller β and with little dependence on Γ for fixed Δ . The functional form becomes more complex at higher Γ , displaying behavior similar to that of environmentally assisted transport^{29,50,51}, with a peak in β with increasing Γ at larger Δ . For example, for $\Delta = 0.1$ a.u. increasing $\Gamma_{C_2} = \Gamma_{D_f}$ from 10^{-6} a.u. to 0.1 a.u. results in an increase in β by almost two orders of magnitude.

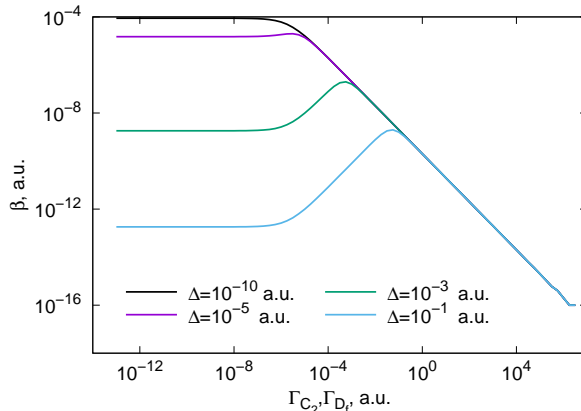


FIG. 2. Variation of the coherence component β of the rate with respect to the parameters Δ and $\Gamma_{C_2} = \Gamma_{D_f}$ in the V-system.

B. Grouped V-system model

As an example of the flexibility of the methodology, consider the case where $|g\rangle$ and $|1\rangle$ are grouped together and where the population transfer between this group and state 2 is of interest (Fig. 1). This constitutes a totally different definition of the components within

the network than that considered above. To do so we redefine the projectors to construct a network for two groups rather than three via the projectors $\hat{P}_A = |g\rangle\langle g| + |1\rangle\langle 1|$ and $\hat{P}_2 = |2\rangle\langle 2|$. Doing so describes a network in terms of the populations $p_A = \rho_{gg} + \rho_{11}$ and p_2 , with the NESS rates between the two groups in this network given as (see Appendix C for a derivation)

$$k_{2A} = 2 \frac{(\Gamma_{H_1} + \Gamma_{H_2})(\beta + \Gamma_{D_f}) + \Gamma_{H_2}\Gamma_{C_1}}{r(\beta + \Gamma_{D_f}) + \Gamma_{H_1} + (1-r)\Gamma_{H_2} + \Gamma_{C_1}}, \quad (29)$$

$$k_{A2} = 2 \frac{\left\{ \begin{aligned} &(\beta + \Gamma_{D_f} + \Gamma_{H_1} + \Gamma_{C_1})\Gamma_{C_2} \\ &+ (\beta + \Gamma_{D_b})(\Gamma_{H_1} + \Gamma_{H_2} + \Gamma_{C_1}) \end{aligned} \right\}}{r(\beta + \Gamma_{D_f}) + \Gamma_{H_1} + (1-r)\Gamma_{H_2} + \Gamma_{C_1}}, \quad (30)$$

where r is a ratio of the ground state population within group A in the non-equilibrium steady state [here denoted by superscript s],

$$r = \frac{\rho_{gg}^{(s)}}{\rho_{gg}^{(s)} + \rho_{11}^{(s)}}. \quad (31)$$

a quantity that generally depends on all parameters. These rates completely account for the coherence ρ_{12} and the internal state of group A , described by $(1-r)\rho_{gg} - r\rho_{11}$ (see Appendix C) in the steady state. The parameter dependence of the rates is totally different than the three level V-system discussed above, and is too complicated to allow us to assess conditions under which $k_{2A} > k_{A2}$, driving population onto state 2, or $k_{2A} < k_{A2}$, the reverse.

The key difference between the rate in the grouped model compared to that in the standard V-system is the role played by the hot bath. In the latter case, the NESS rates between excited states do not depend on \mathcal{L}_H , whereas rates in the grouped model are directly influenced by the hot bath. For example, the forward rate from group A to state 2 in the latter case is zero if $\mathcal{L}_H = 0$.

The significance of the hot bath in the grouped model can be understood by noting that forward population transfer can occur via two mechanisms: (1) population transfer from state g to state 2 through the term Γ_{H_2} , and (2) population transfer from state 1 to state 2 through the term $(\beta + \Gamma_{D_f})$. Both mechanisms, and hence the rate to state 2, involve the hot bath, the first explicitly and the second implicitly since it requires state 1 to be populated. The interplay of k_{2A} and the external parameters $\Gamma_{H_1}, \Gamma_{H_2}$ is far from trivial and is shown in Fig. 3a. However, it is clear that for $\Gamma_{H_2} = 0$ and $\Gamma_{H_1} < 10^{-4}$, the forward rate k_{2A} increases near-linearly as a function of Γ_{H_1} .

As for the backward rate k_{A2} , it also depends on \mathcal{L}_H but this rate is non zero even when $\mathcal{L}_H = 0$ as can be seen in Fig. 3b and understood from Eq. (30) by setting $\Gamma_{H_1} = \Gamma_{H_2} = 0$ and using the fact that $r = 1$ in this limit:

$$\lim_{\Gamma_{H_1}, \Gamma_{H_2} \rightarrow 0} k_{A2} = 2 \left(\Gamma_{C_2} + \frac{(\beta + \Gamma_{D_b})\Gamma_{C_1}}{\beta + \Gamma_{D_f} + \Gamma_{C_1}} \right). \quad (32)$$

Two processes are clearly seen in this last equation: direct population transfer from state 2 to the ground state through Γ_{C_2} , and the two-step population transfer going through state 1.

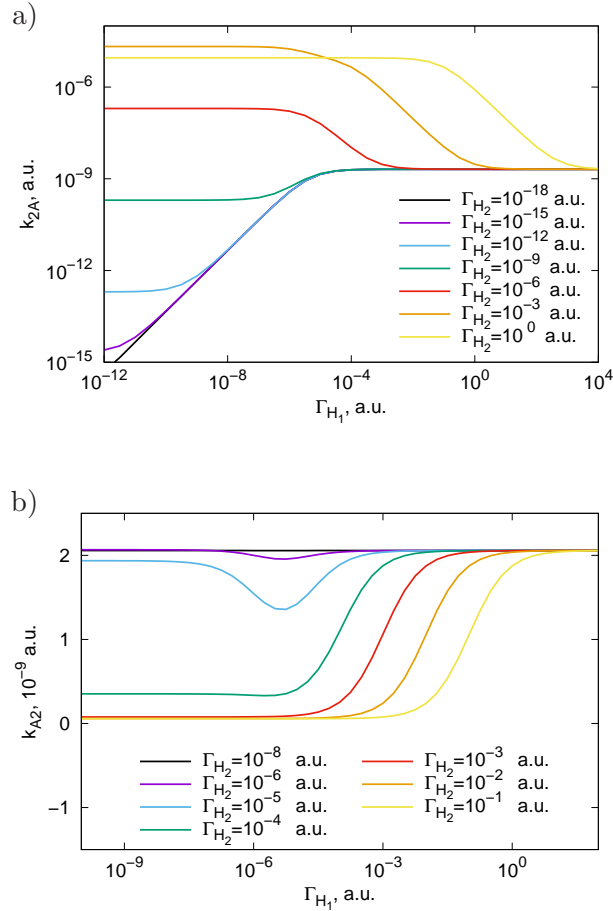


FIG. 3. Variation of (a) the forward rate k_{2A} , and (b) the backward rate with respect to the parameters Γ_{H_1} and Γ_{H_2} in the grouped V-system model.

An interesting feature of both rates, which can be observed in Figs. 3a and 3b, is that they are both bound in the limit of large Γ_{H_1} or Γ_{H_2} . This effect can be simply exposed by

taking the appropriate limits of Eqs. (29-30) and using the fact that $r = 0$ in this limit:

$$\lim_{\Gamma_{H_1} \rightarrow \infty} k_{2A} = 2(\beta + \Gamma_{D_f}), \quad (33)$$

$$\lim_{\Gamma_{H_2} \rightarrow \infty} k_{2A} = 2(\beta + \Gamma_{D_f} + \Gamma_{C_1}), \quad (34)$$

$$\lim_{\Gamma_{H_1} \rightarrow \infty} k_{A2} = 2(\beta + \Gamma_{D_b} + \Gamma_{C_2}), \quad (35)$$

$$\lim_{\Gamma_{H_2} \rightarrow \infty} k_{A2} = 2(\beta + \Gamma_{D_b}). \quad (36)$$

A comparison of these rates with Fig. 1 shows how taking the limit of specific large radiative pumping Γ_{H_1} or Γ_{H_2} highlights specific pathways for population transfer in the grouped V-system. However, even for a strong external perturbations the maximal rate is limited by the cold bath and by the system itself.

In typical natural systems the radiative pumping rate is very small, in which case k_{2A} is proportional to $\Gamma_{H_1} + \Gamma_{H_2}$, which is then the rate determining step.

IV. NONEQUILIBRIUM SPIN-BOSON MODEL

As a second example consider now a more general case of a composite system that contains both nuclear and electronic degrees of freedom coupled to two baths. The system chosen is the spin-boson model⁵², which provides input into such important processes as *cis-trans* isomerization in the first steps in vision⁵³ and proposed photoswitches⁵⁴.

The system Hamiltonian in the diabatic electronic basis is given by

$$\begin{aligned} \hat{H}_S = \sum_{k=1}^2 \left[\left(-\frac{\Omega_k}{2} \frac{\partial^2}{\partial \hat{q}^2} + \frac{\Omega_k}{2} (\hat{q} - q_k)^2 + \epsilon_k \right) |k\rangle \langle k| \right] \\ + \lambda (|1\rangle \langle 2| + |2\rangle \langle 1|), \end{aligned} \quad (37)$$

where k indexes the electronic state (either 1 or 2), \hat{q} is the vibrational coordinate, Ω_k is the frequency of the oscillator in the k^{th} electronic state, and q_k and ϵ_k are the horizontal and vertical displacements respectively, and the system is subjected to incident incoherent light. Figure 4 provides a representative example of the system considered.

The diabats are coupled to a common cold phonon bath (ph) and to a hot thermal bath (rad) used to mimic incoherent radiation-induced transitions between the two diabats. Both baths are given in the Lindblad form. It assumes that the behavior is Markovian, which is

exact in the case of the NESS. The master equation for the system excited by incoherent radiation is then given as

$$\dot{\hat{\rho}} = -i[\hat{H}_S, \hat{\rho}] + \sum_{\nu=\{\text{rad,ph1,ph2}\}} \mathcal{L}_\nu[\hat{\rho}], \quad (38)$$

with

$$\begin{aligned} \mathcal{L}_\nu[\hat{\rho}] = & \Gamma_\nu(n_\nu + 1) \left(\hat{S}_\nu \hat{\rho} \hat{S}_\nu^\dagger - \frac{1}{2} [\hat{S}_\nu^\dagger \hat{S}_\nu, \hat{\rho}]_+ \right) \\ & + \Gamma_\nu n_\nu \left(\hat{S}_\nu^\dagger \hat{\rho} \hat{S}_\nu - \frac{1}{2} [\hat{S}_\nu \hat{S}_\nu^\dagger, \hat{\rho}]_+ \right). \end{aligned} \quad (39)$$

Here Γ_ν scales the interaction of the bath, n_ν gives the mean number of excitations, and \hat{S}_ν are system operators in the combined nuclear-electronic subspace responsible for the coupling to the baths, defined below. The mean number of excitation is defined as $n_\nu = (\exp(\frac{E_\nu}{k_B T_\nu}) - 1)^{-1}$ where k_B is the Boltzmann constant, T_ν is the temperature of the corresponding bath, and E_ν is the level spacing of the corresponding bath i.e. $E_{ph,k} = \Omega_k$ and E_{rad} is the energy gap between the two diabats at $q = -3$. The radiation bath directly couples electronic states via dipole coupling, i.e.,

$$\hat{S}_{\text{rad}} = |1\rangle\langle 2|, \quad (40)$$

while the phonon bath is coupled to each diabatic state k as

$$\hat{S}_{\text{ph},k} = \left(\hat{a} - \frac{q_k}{\sqrt{2}} \right) |k\rangle\langle k|. \quad (41)$$

Here $\hat{a} = \frac{1}{\sqrt{2}}(\hat{q} + \frac{\partial}{\partial \hat{q}})$ and $\hat{S}_{\text{ph},k}$ is the annihilation operator of the oscillator defined in state k . The specific form of dissipators is that of a local quantum master equation⁵⁵⁻⁵⁷ such that the chosen model is valid in the weak coupling limit.

As one partitioning example we identify the rate of interest as that at which population is transferred from the left to the right of a dividing surface (see Fig. 4), chosen to lie at the intersection created between the two diabats denoted q_X . Note that this rate is analogous to that commonly used to study molecular reactions within the reactive flux formalism. This situation is also reminiscent of the study of *cis-trans* isomerization in retinal⁵³ in which the crossing of the dividing surface corresponds to the system undergoing isomerization from the *cis* to the *trans* configuration. These rates are defined via the Hilbert space projectors

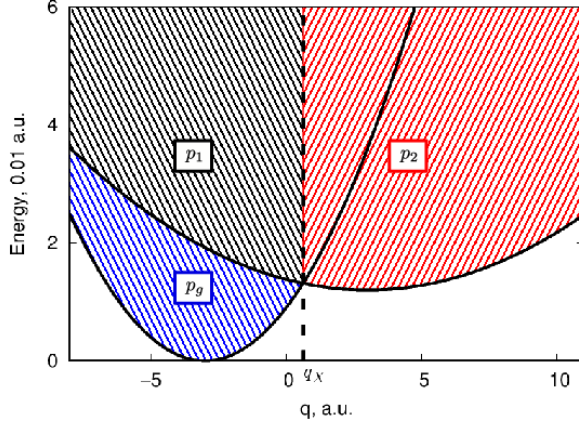


FIG. 4. Depiction of the nonequilibrium spin boson model. The dashed line indicates the dividing surface used to partition the nuclear coordinate q , defining the position q_X . The hatch patterns depict the partition defined in Eqs. (46-48).

that satisfy Eqs. (5) and (6) as

$$\hat{P}_L = \int_{-\infty}^{q_X} dq |q\rangle \langle q|, \quad (42)$$

$$\hat{P}_R = \int_{q_X}^{\infty} dq |q\rangle \langle q|. \quad (43)$$

For a numerical example, parameters (in atomic units) are taken as follows unless otherwise stated: $\Omega_1 = 2 \times 10^{-3}$, $\Omega_2 = 4 \times 10^{-4}$, $\epsilon_2 - \epsilon_1 = 0.012$, $q_1 = -3.0$, $q_2 = 3.0$, $\lambda = 2 \times 10^{-5}$, $\Gamma_{rad} = 10^{-6}$, $\Gamma_{ph,1} = \Gamma_{ph,2} = 10^{-9}$, radiation bath temperature $T_{rad} = 5800K$ and phonon bath temperature $T_{ph} = 300K$.

Computations are done by projecting all the operators onto a basis comprised of a direct product of the electronic and nuclear bases, where the nuclear coordinate basis is chosen as harmonic oscillators centered at $q = 0$ a.u. (i.e. eigenstates of $\hat{q}^2 - \partial^2/\partial q^2$). We use a large nuclear basis of 400 basis functions to properly represent the projector operators \hat{P}_R and \hat{P}_L . In order to reduce the computational cost, the large basis must be truncated, while preserving the partition given by the projectors. To achieve this goal we diagonalize the localized Hamiltonians $\hat{P}_R \hat{H}_s \hat{P}_R$ and $\hat{P}_L \hat{H}_s \hat{P}_L$ and retain only eigenstates that are lower in energy than $50\Omega_2 + \epsilon_2 - \epsilon_1$. We then vectorize the steady state Liouville equation and solve the linear problem of Appendix A using standard linear algebra routines.

Processes like this, e.g. molecular isomerization, are often studied with ultrafast laser pulses³². For this reason, the rate following a vertical excitation is also of interest. This is computed by first turning off the photon bath (setting $\Gamma_{rad}=0$) and obtaining the stationary

density ρ_s . This density is then excited using a high order perturbation expansion⁵⁸ to obtain the vertically excited state:

$$\rho_{\text{VE}} = \rho_s + \lim_{n \rightarrow \infty} \sum_{k=1}^{\infty} \rho_k \quad (44)$$

Here ρ_k is defined via k nested commutators:

$$\rho_k = \left(-\frac{i}{\hbar} \right)^k [\mu, [\mu, \dots, [\mu, \rho_s] \dots]]_k, \quad (45)$$

$\mu = \alpha|2\rangle\langle 1| + \text{h.c.}$ with $\alpha = 0.45$ modeling the strength of the dipole in the perturbation expansion. The resultant excitation is ~ 0.5 eV. The density is then evolved in time to calculate the transfer rate from one side of the dividing surface to the other.

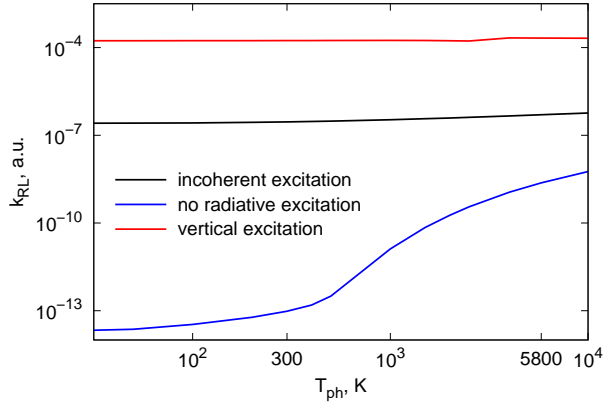


FIG. 5. Dependence of the forward rate with incoherent excitation (black), vertical excitation (red), and no radiative transition (blue) when varying T_{ph} .

It is well established (e.g., see Refs. 59 and 33), but often ignored, that rates of radiatively excited processes depend intimately on the nature of the incident light. Figure 5 displays the behavior of (a) the forward NESS rate, (b) the rate following the dynamics after a vertical excitation and (c) the rate with no excitation radiative (only phonon bath effects), all with respect to the phonon bath temperature T_{ph} . The three rates are seen to occur with vastly different magnitudes. The fastest rate, 10^{-4} a.u. $\sim 10^{-2}$ fs⁻¹, is that obtained via vertical excitation. This rate does not depend on the phonon bath temperature since the vertical excitation energy of ~ 0.5 eV is much larger than phonon bath effects, which only transfer small amounts of population. Even at the highest temperature shown in Fig. 5, excitation due to thermal fluctuations are minuscule compared to that of the vertical excitation.

Figure 5 shows that the NESS rate with incoherent excitation is ~ 3 orders of magnitude smaller than that of vertical excitation for nearly all temperatures. The magnitude of this rate is seen to be nearly independent of the phonon bath for the parameter set of the incoherent light sources considered here due to the difference in energy scales. Significantly, the vertical excitation rate, similar to that achieved in pulsed laser experiments, is orders of magnitude faster than the incoherent excitation NESS rate, reinforcing the view^{33,60} that rates from pumped laser experiments do not reflect time scales under normal incoherent light.

Finally, the rate with no radiative excitation is relevant to, e.g., thermally induced *cis-trans* isomerization of rhodopsin⁶¹. It is, as expected, the slowest. Here, with system in the dark, the rate of population transfer is independent of the phonon temperature and is very small until $\sim 1000K$. At this point (attenuation factor of 0.47) there is enough thermal energy to overcome the barrier that separates the two minima. Such an effect is only evident in the absence of radiative contributions. Even when the temperature of the phonon bath approaches that of the photon bath at $5800K$ there is a large difference between the thermal rate and the radiative rates. This is mainly due to the fact that, unlike the phonon bath, radiation couples electronic states directly through dipolar coupling, which allows them to transfer population without having to cross a barrier.

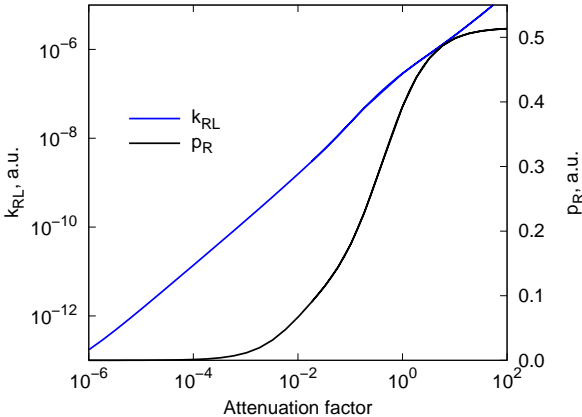


FIG. 6. Dependence of the forward rate and the transferred population on the photon attenuation factor α .

Molecules on earth do not experience the full strength of the solar spectrum due to absorption by the atmosphere. Additional attenuation occurs due to artificial or cloud cover,

or light absorption by water for undersea plants. To simulate the attenuation of the incident incoherent light of the radiative bath, we introduce an attenuation factor α and replace n_{rad} by the effective quantity αn_{rad} . As seen in Fig. 6 the dependence of the forward rate on the attenuation factor is linear on a log-log plot. This is indicative of power law dependence, and a least square analysis shows that the rate depends approximately linearly on n_{rad} . Hence, when light is attenuated by $\alpha = 10^{-2}$, the rate is also reduced by a factor of 10^{-2} . (Realistic attenuation factors in some photosynthetic systems can be smaller⁴⁹ than 10^{-7} .) This is expected since, under strong attenuation only few photons excite the system to allow for the subsequent population transfer. Indeed, for a low attenuation factor most of the system is in the first electronic state and populates low energy states localized on the left of the dividing surface (see the transferred population in Fig 6). By unphysically increasing α , we can reach a NESS rate that is as large as the rate obtained with a vertical excitation. However, such a large value $\alpha \sim 10^2$ implies a huge unphysical radiation temperature $T \sim 3 \times 10^5$ K.

One further note about this scenario is in order. The comparative behavior of the forward rate and the transferred population, seen in Fig. 6, is also enlightening. In particular, the transferred population follows the attenuation factor at small α . However, the transferred population increases dramatically after $\alpha \approx 10^{-2}$, reaching a maximum of ≈ 0.5 after $\alpha \approx 10$. This behavior may well be of interest to experiments designing materials operating in, e.g., a solar furnace where temperatures can reach 3000 degrees K. In our case the behavior arises as follows: When the attenuation factor is small, most population is in the lowest energy states, which are located on the left side. As the incoming energy reaches the energy of the lowest state located on the right side (0.012 a.u., equivalent to a temperature of 3800K), these states become significantly populated. At this point the population starts to grow dramatically. When the incoming energy is much larger than 0.012 a.u., both left and right states become equally populated, with the transferred population tending to a limit of 0.5. This type of behavior is clearly system dependent, and can certainly occur at lower temperatures, depending on system eigenstates.

The general behavior of this system resembles that of the grouped V-system in displaying a dependence on the external driving field. Such rates, where a weak excitation step is included in the overall system definition, correctly identifies the excitation as the rate determining step in the production of the final state. They have been studied in detail for processes like energy transfer in LH1⁴⁹ and the initial steps in vision²⁶⁻²⁸. However, the ap-

proach introduced here allows different choices of projection operators, and hence different partitioning of the network. This allows us *a focus on the dynamics of the process within the excited state, a quantity giving insight into the rate of population transfer post excitation that is independent of the excitation.* This approach is reminiscent of the (ungrouped) V-system above.

To extract the rate independent of the excitation step we partition the system into three components through the following projection operators (see Fig. 4):

$$\hat{P}_g = \hat{P}_L|1\rangle\langle 1|, \quad (46)$$

$$\hat{P}_1 = \hat{P}_L|2\rangle\langle 2|, \quad (47)$$

$$\hat{P}_2 = \hat{P}_R. \quad (48)$$

Here \hat{P}_g projects onto the lower electronic state on the left side and \hat{P}_1 onto the upper electronic state on the left side. These choices subdivide the system between parts that exchange population through the radiative bath if we assume that most of the population is located on the left side. The projector \hat{P}_2 is chosen as \hat{P}_R , i.e., we do not split the electronic states on the right side because we assume, for the chosen parameters, that electronic state 1 will be only weakly populated in this region. Numerical results are obtained using the same methodology as described above, and resultant rates are shown in Fig. 7. They clearly display a forward rate, k_{21} which, for $\alpha < 10^{-2}$, does not depend on the radiative bath.

This lack of dependence of k_{21} on the attenuation is similar to that observed in the ungrouped V-system case in Sec. III, indicative of the fact that the excitation step has been properly separated from the excited state dynamics within the network. This is a significant result, allowing deep insight into the flow of population internal to the network.

V. RATES AND THE DEVIATION FROM THE NESS

The above results pertain to the all-important NESS region. When the system is perturbed out of the NESS, the population dynamics are not expected to be described by the rate equation. However, there are situations where the range of validity of the NESS kinetic equations extends outside the NESS regime. This is of particular relevance in determining when one can extend to the NESS, a practice common for equilibrium cases, where equilibrium rates are obtained from the rate of return of a perturbation back to equilibrium^{62,63}.

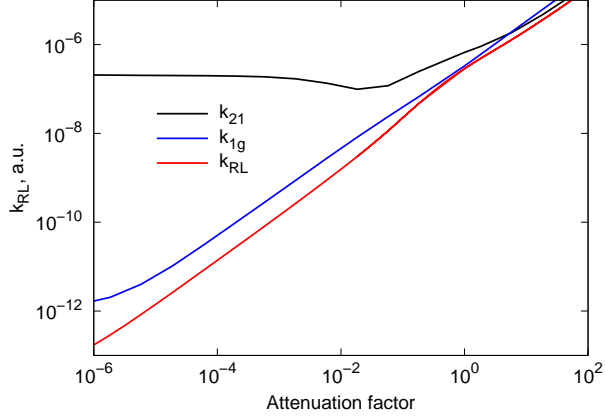


FIG. 7. Dependence of the rates k_{1g} and k_{21} on the attenuation factor α in the case of the partition into three components. The rate k_{RL} is given for the purpose of comparison.

Interestingly, as shown below, conditions where this is the case are intimately related to the role of Markovian vs. non-Markovian contributions to Eq. (13). Note that these contributions arise from separating the population dynamics from the complementary Liouville space, and do not refer to the Markovianity or non-Markovianity of the bath. Here we introduce these conditions and provide an application to the V-system.

Consider then Eq. (13), which can be partitioned into two terms

$$\dot{\mathbf{p}} = \mathbf{M}^{(1)} + \mathbf{M}^{(2)} \quad (49)$$

where the first term, $\mathbf{M}^{(1)}$ is the contribution from the NESS rates defined in Eq. (15),

$$M_m^{(1)} = \sum_{n=1}^N k_{mn} p_n. \quad (50)$$

This $M^{(1)}$ term generates Markovian evolution since the generator k_{mn} does not contain memory terms. The $\mathbf{M}^{(2)}$ term is then the difference $\dot{\mathbf{p}} - \mathbf{M}^{(1)}$:

$$\begin{aligned} M_m^{(2)} &= \text{Tr}\{\hat{P}_m \mathcal{L} e^{\mathcal{Q}\mathcal{L}\mathcal{Q}t} \mathcal{Q}[\hat{\rho}(0)]\} + \sum_{n=1}^N \int_0^t d\tau \text{Tr}\{\hat{P}_m \mathcal{L} e^{\mathcal{Q}\mathcal{L}\mathcal{Q}(t-\tau)} \mathcal{Q}\mathcal{L}[\hat{\rho}_n]\} p_n(\tau) \\ &+ \sum_{n=1}^N \text{Tr}\{\hat{P}_m \mathcal{L} (\mathcal{Q}\mathcal{L}\mathcal{Q})^{-1} \mathcal{Q}\mathcal{L}[\hat{\rho}_n]\} p_n. \end{aligned} \quad (51)$$

This term contains the time integral memory component and depends on the initial condition $\mathcal{Q}[\hat{\rho}(0)]$, and hence generates non-Markovian dynamics. For the derived kinetic

equations to be accurate away from NESS, the non-Markovian terms need to be negligible. The Markovian approximation, which characterizes the NESS, applies if after some transient dynamics of duration $t^{(2)}$ the terms of $\mathbf{M}^{(2)}$ vanish. Similarly, we can define the time t_s which is required for the system to reach the steady state. If $t_s \gg t^{(2)}$, then the populations follow the kinetic equations (or Markovian dynamics) for the time range $t \in [t^{(2)}, t_s]$. The population dynamics during this time range can be used, if desired, to extract the rates by employing a fitting procedure without calculating them using Eq. (15). However, if $t^{(2)} > t_s$, this rate extraction is not possible since the Markovian approximation is not valid for any time $t < t_s$. (In either case, however, the NESS rates can, of course, be obtained via Eq. (15).)

Consider then the timescales $t^{(1)}$ and $t^{(2)}$, which can be estimated as follows: $t^{(2)}$, is dictated by the decay of $e^{\mathcal{Q}\mathcal{L}\mathcal{Q}t}$. Hence we define the eigenvalues of $\mathcal{Q}\mathcal{L}\mathcal{Q}$ and order them as $0 > \text{Re}[\kappa_1^{(2)}] > \text{Re}[\kappa_2^{(2)}] > \dots > \text{Re}[\kappa_n^{(2)}] \dots$. The slowest decay process $e^{\kappa_1^{(2)}t}$ then determines $t^{(2)} = 1/\text{Re}[\kappa_1^{(2)}]$ a.u. Once $\mathbf{M}^{(2)}$ becomes negligible, the populations exponentially decay as $\mathbf{p}(t) = e^{\mathbf{k}(t-t^{(2)})}\mathbf{p}(t^{(2)})$. Hence, this timescale is also governed by an exponential decay and using the eigenvalues of the matrix \mathbf{k} , we order them as $0 > \kappa_1^{(1)} > \kappa_2^{(1)} > \kappa_3^{(1)} \dots$. The slowest decay process $e^{\kappa_1^{(1)}t}$ determines $t^{(1)}$, which we define as $t^{(1)} = 1/\text{Re}[\kappa_1^{(1)}]$ a.u. With these definitions, the dynamics is Markovian if $t^{(2)} \ll t^{(1)}$ and the kinetic rate equations are valid in this time domain.

To gain insight into this analysis, and obtain these time scales for a given system, we could calculate the exact dynamics and extract the time evolution of both terms. The exact dynamics would be obtained by exponentiation of the Liouvillian from a perturbed initial state. The resulting density matrix and its time-derivative would then be used to extract $\mathbf{p}(t)$ and $\dot{\mathbf{p}}(t)$ at various times. A detailed study of $t^{(2)}$, $t^{(1)}$ and t_s is the subject of future work, Here we provide one example based on the models introduced above.

Consider the case of the V-system in Sec. III. The parameters given in Table I give the time scale estimates $t^{(1)} = 4.0 \times 10^8$ and $t^{(2)} = 6.6 \times 10^5$ a.u.

Since $t^{(2)} \ll t^{(1)}$, we anticipate that the dynamics after time $t^{(2)}$ will be Markovian and essentially driven by the first term $\mathbf{M}^{(1)}$. Indeed, this is what is observed in Fig. 8a where $\mathbf{M}^{(2)} \ll \mathbf{M}^{(1)}$ after the time $t^{(2)}$. Since $t^{(2)}$ is an order of magnitude smaller than $t^{(1)}$, the dynamics is expected to follow an exponential decay on the global timescale, whose generator is \mathbf{k} . This is indeed what is observed in Fig. 8b where the population dynamics

obtained from the model given by the steady state rates is compared to the exact dynamics. This difference can be quantified by calculating the relative error

$$\frac{2 \int_{t^{(2)}}^{t_f} \|\dot{\mathbf{p}}(t) - \mathbf{k}\mathbf{p}(t)\| dt}{\int_{t^{(2)}}^{t_f} \|\dot{\mathbf{p}}(t) + \mathbf{k}\mathbf{p}(t)\| dt}, \quad (52)$$

where t_f is the final propagation time. Using a time step $\delta t \approx 7 \cdot 10^4$ a.u., the obtained relative error is 7.2×10^{-2} . We can also extract the rates that would fit best the population curves by minimizing $\int_{t^{(2)}}^{t_f} \|\dot{\mathbf{p}}(t) - \mathbf{k}\mathbf{p}(t)\|^2 dt$ on the time grid. The resulting linear equation to solve in order to obtain the fit transition rate matrix is

$$\mathbf{k}_{fit} = \int_{t^{(2)}}^{t_f} \dot{\mathbf{p}}(t)\mathbf{p}^T(t) dt \left[\int_{t^{(2)}}^{t_f} \mathbf{p}(t)\mathbf{p}^T(t) dt \right]^{-1}, \quad (53)$$

where the superscript T denotes the transpose. Eigenvalues of \mathbf{k}_{fit} , $\{0, 0, -2.58 \cdot 10^{-9}\}$, can be compared to the eigenvalues of \mathbf{k} , $\{0, -2.58 \cdot 10^{-9}, -1.21 \cdot 10^{-5}\}$. Hence, the long timescale is quantitatively recovered from the fitting procedure with an error of less than 10%.

The alternative situation arises when J [and hence the coherence mediated rate β in Eq. (24)] is increased. This is a signature of the importance of the complementary space, which can be quantified by the spectral norm $\|[\mathcal{QLQ}]^{-1}\|$ in Eq. (15). This is indeed what we observe when we set $J = 0.02$ a.u. and obtain $\text{Re}[\kappa_1^{(2)}] = -3.3 \times 10^{-6}$ a.u. In this case, the timescale for $\mathbf{M}^{(2)}$ is given by $t^{(2)} = 3.0 \times 10^5$ a.u. and the $\mathbf{M}^{(1)}$ timescale gives $t^{(1)} = 1.4 \times 10^5$. As a result, $t^{(1)} < t^{(2)}$ and $\mathbf{M}^{(1)} < \mathbf{M}^{(2)}$ for the entire dynamics. Thus, $\mathbf{M}^{(2)}$ is never negligible and non-Markovianity dominates for all times, as seen in Fig. 9a. The same conclusion is reached by observing the population dynamics in Fig. 9b. In this case, the relative error defined in Eq. (52) is 2, so that it is impossible to define a time-range over which rates can be extracted to fit the dynamics. That is, the NESS rates have to be properly determined from Eq. (15). This can already be understood by visual inspection of Fig. 9b, where the populations p_1 and p_2 are oscillating during the entire time evolution.

It is clear then that there are circumstances under which perturbations away from the NESS can be used to obtain information on rates within the NESS. These results motivate further, ongoing, work to examine the possibility of identifying physical conditions under which the Markovian or non-Markovian dynamics applies as a system approaches the NESS, and hence useful conditions for the utility of perturbations away from the NESS to determine internal rates.

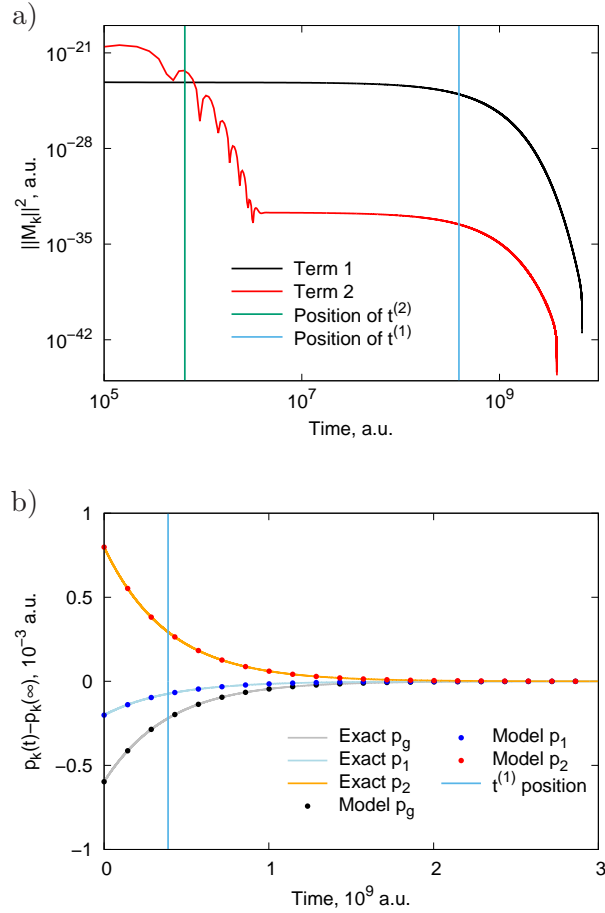


FIG. 8. Time evolution for the V-system in the Markovian case. (a) $\mathbf{M}^{(1)}$ and $\mathbf{M}^{(2)}$ and (b) the populations comparing exact propagation to steady state rates .

VI. CONCLUSION AND FUTURE WORK

We have presented a rigorous methodology for defining components of a network via projection operators, and for obtaining rates of population flow between these components in the all important non-equilibrium steady state (NESS). Quantum effects are included both via the projection operators as well as in the incorporation of coherences. The versatile projection operator formalism allows, for example, the removal of the rate of weak radiative absorption, typically the rate determining step, exposing the rates within the excited states.

The NESS rates defined in this formalism are not based on the commonly used linear response formalism⁶⁴ and are valid in all parameter regimes. In addition, our approach has allowed insights into the temporal range of utility of the kinetic network away from the NESS, in terms of Markovian and non-Markovian contributions to the time evolution of the

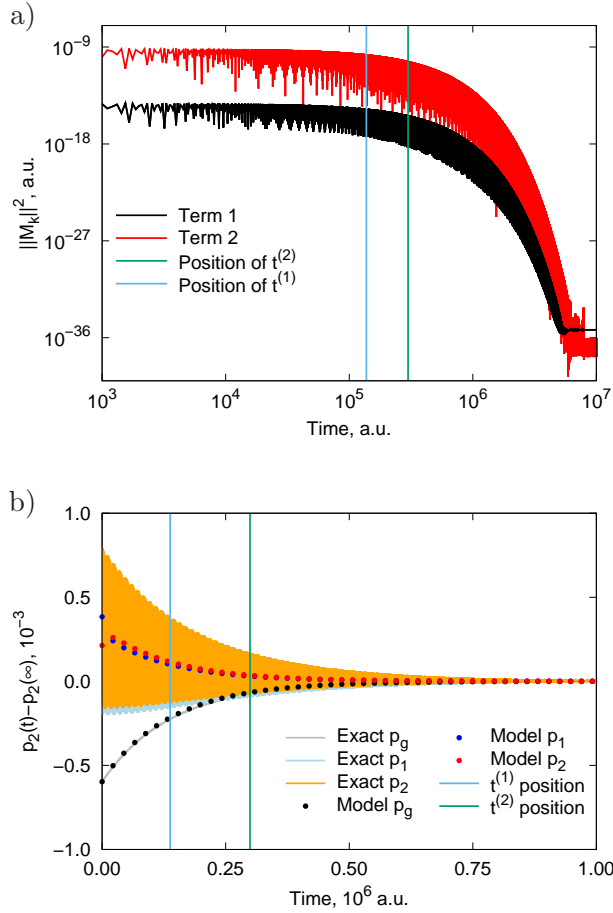


FIG. 9. Time evolution of the V-system in the non-Markovian case. (a) $\mathbf{M}^{(1)}$ and $\mathbf{M}^{(2)}$ and (b) the populations comparing exact propagation and steady state rates .

populations. This constitutes significant input into the issue of when the NESS rates can be determined by perturbing the system away from the NESS. Finally, note that while the examples presented make use of the Lindblad description of open systems, the methodology is completely general and can be straightforwardly applied to any description of the Liouville equation, such as Redfield theory^{65,66} or, ideally, the exact Zwanzig-Nakajima form.

The formalism developed has allowed us to analyze two commonly used population transfer models, the V-system and the nonequilibrium spin-boson model, giving further insight into the behavior of the NESS rates. Both cases where the excitation step is included or excluded were examined. In addition, the application to the nonequilibrium spin-boson model with no attenuation of the incident light, showed that the rate obtained via vertical excitation is approximately three orders of magnitude larger than the NESS rate. This finding supports the view (for a review see Ref. 33) that ultra-fast experiments that probe systems

that operate naturally under NESS conditions are, in fact, preparing and observing system dynamics that are totally different from those that occur naturally.

The NESS rates discussed in this work are a major step forward, since they characterize the rate under proper, natural, NESS conditions, where the network definition is general. Future work will explore these effects in biologically motivated models such as the Hahn-Stock retinal model.⁶⁷ Currently the method relies on the inversion of a Liouville superoperator which is computationally memory intensive for even modestly sized systems. Future work will focus on ways to alleviate this bottleneck, such as the iterative scheme in Ref.²⁷, so that the rate calculation can be applied to larger systems. In addition to overcoming the computational challenges, the formal connections to other aspects of rate theory will be further explored.

ACKNOWLEDGMENTS

This material is based upon work supported by the U.S. Air Force Office of Scientific Research under award number FA9550-20-1-0354.

Appendix A: Rates by solving a linear equation

A simple way to obtain the rates defined by Eq. (15) is by solving the system of linear Eqs. (10-11) in the steady state limit. Taking Eq. (11) for $\rho = \rho_s$, we obtain the linear equation to solve for $\mathcal{Q}[\rho_s]$

$$0 = \sum_{n=1}^N \mathcal{Q}\mathcal{L}[\varrho_n]p_n + \mathcal{Q}\mathcal{L}\mathcal{Q}[\rho_s]. \quad (\text{A1})$$

Writing the solution as

$$\mathcal{Q}[\rho_s] = - \sum_{n=1}^N (\mathcal{Q}\mathcal{L}\mathcal{Q})^{-1} \mathcal{Q}\mathcal{L}[\varrho_n]p_n. \quad (\text{A2})$$

we can substitute it for $\mathcal{Q}[\rho_s]$ in Eq. (10), and obtain

$$\begin{aligned} \dot{p}_m &= \sum_{n=1}^N \text{Tr}\{\hat{P}_m \mathcal{L}[\hat{\varrho}_n]\}p_n \\ &\quad - \sum_{n=1}^N \text{Tr}\{\hat{P}_m \mathcal{L}(\mathcal{Q}\mathcal{L}\mathcal{Q})^{-1} \mathcal{Q}\mathcal{L}[\varrho_n]\}p_n, \end{aligned} \quad (\text{A3})$$

which is in fact Eq. (14) with our rate definition of Eq. (15).

Appendix B: Rates in the V-system

Starting from Eq. (20), we wish to derive Eqs. (21-23) in the steady state limit. We proceed by solving the system of linear equations (Eqs. 10-11) for the populations $\{\rho_{nm}\}$ in the steady state limit (similar to Appendix A). Taking matrix elements of Eq. (20), we obtain a set of equations for each element of the density matrix:

$$\text{Tr}\{\hat{P}_g\dot{\hat{\rho}}\} = \dot{\rho}_{gg} = -2(\Gamma_{H_1} + \Gamma_{H_2})\rho_{gg} + 2\Gamma_{C_1}\rho_{11} + 2\Gamma_{C_2}\rho_{22}, \quad (\text{B1})$$

$$\text{Tr}\{\hat{P}_1\dot{\hat{\rho}}\} = \dot{\rho}_{11} = -iJ(\rho_{21} - \rho_{12}) + 2\Gamma_{H_1}\rho_{gg} - 2(\Gamma_{C_1} + \Gamma_{D_f})\rho_{11} + 2\Gamma_{D_b}\rho_{22}, \quad (\text{B2})$$

$$\text{Tr}\{\hat{P}_2\dot{\hat{\rho}}\} = \dot{\rho}_{22} = -iJ(\rho_{12} - \rho_{21}) + 2\Gamma_{H_2}\rho_{gg} - 2(\Gamma_{C_2} + \Gamma_{D_b})\rho_{22} + 2\Gamma_{D_f}\rho_{11}, \quad (\text{B3})$$

$$\langle g | \mathcal{Q}[\dot{\hat{\rho}}] | 1 \rangle = \dot{\rho}_{g1} = i(\epsilon_1 - \epsilon_g)\rho_{g1} - (\Gamma_{H_1} + \Gamma_{H_2} + \Gamma_{C_1} + \Gamma_{D_f})\rho_{g1} + iJ\rho_{g2}, \quad (\text{B4})$$

$$\langle g | \mathcal{Q}[\dot{\hat{\rho}}] | 2 \rangle = \dot{\rho}_{g2} = i(\epsilon_2 - \epsilon_g)\rho_{g2} - (\Gamma_{H_1} + \Gamma_{H_2} + \Gamma_{C_2} + \Gamma_{D_b})\rho_{g2} + iJ\rho_{g1}, \quad (\text{B5})$$

$$\langle 1 | \mathcal{Q}[\dot{\hat{\rho}}] | 2 \rangle = \dot{\rho}_{12} = (i\Delta - \Gamma_{C_1} - \Gamma_{C_2} - \Gamma_{D_f} - \Gamma_{D_b})\rho_{12} + iJ(\rho_{11} - \rho_{22}). \quad (\text{B6})$$

The diagonal terms of $\mathcal{Q}[\dot{\hat{\rho}}]$ are trivially zero since $\langle k | \mathcal{Q}[\dot{\hat{\rho}}] | k \rangle = 0$, and equations for other elements can be obtained directly since $\hat{\rho}$ is Hermitian: $\rho_{1g} = \rho_{g1}^*$, $\rho_{2g} = \rho_{g2}^*$, $\rho_{21} = \rho_{12}^*$.

Note first that the elements ρ_{g1} and ρ_{g2} are completely decoupled from the other elements. Second, from Eq. (B6) and its complex conjugate we can express $\rho_{12} - \rho_{21}$. We isolate ρ_{12} as

$$\rho_{12} = \frac{\dot{\rho}_{12} - iJ(\rho_{11} - \rho_{22})}{i\Delta - \Gamma_{C_1} - \Gamma_{C_2} - \Gamma_{D_f} - \Gamma_{D_b}}. \quad (\text{B7})$$

In the limit of a steady state, we have that $\dot{\rho}_{12} = 0$, which simplifies the expression for ρ_{12} :

$$\rho_{12} = \frac{iJ(\rho_{11} - \rho_{22})}{\Gamma_{C_1} + \Gamma_{C_2} + \Gamma_{D_f} + \Gamma_{D_b} - i\Delta}. \quad (\text{B8})$$

Hence, we have that

$$\rho_{12} - \rho_{21} = \frac{2iJ(\rho_{11} - \rho_{22})(\Gamma_{C_1} + \Gamma_{C_2} + \Gamma_{D_f} + \Gamma_{D_b})}{(\Gamma_{C_1} + \Gamma_{C_2} + \Gamma_{D_f} + \Gamma_{D_b})^2 + \Delta^2}. \quad (\text{B9})$$

Substituting the last expression in Eqs. (B2-B3), we obtain the set of Eqs. (21-23).

The transfer of population between states 1 and 2 is mediated by: (i) the dephasing terms $\{\Gamma_{D_f}, \Gamma_{D_b}\}$ and (ii) by the imaginary part of the coherence ρ_{12} . Interestingly, the time

evolution of ρ_{12} does not depend on Γ_H , see Eq. (B6), since $\langle 1|\mathcal{L}_H|2\rangle = 0$. Hence, ρ_{12} does not depend on Γ_H , nor does the rate between state 1 and state 2.

Note that in the grouping process ρ_{12} is replaced by terms depending on ρ_{11} and ρ_{22} using the time derivative expression of ρ_{12} .

Appendix C: Rates in the grouped V-system

In this section, we demonstrate how to obtain the rates between two groups: group ‘‘A’’, which contains the ground state and state 1, and group 2, which contains only state 2 (as in the previous subsection). Therefore, we define the projectors \hat{I}_A and \hat{I}_2 using the following definitions

$$\hat{P}_2 = |2\rangle\langle 2|, \quad (\text{C1})$$

$$\hat{P}_A = |g\rangle\langle g| + |1\rangle\langle 1|, \quad (\text{C2})$$

$$\hat{\rho}_2 = \hat{P}_2, \quad (\text{C3})$$

$$\hat{\rho}_A = \sum_{kl \in \{g,1\}} |k\rangle \frac{\rho_{kl}^{(s)}}{\rho_{gg}^{(s)} + \rho_{11}^{(s)}} \langle l|. \quad (\text{C4})$$

$$(\text{C5})$$

To simplify the derivation, we have in the steady state, $\rho_{g1}^{(s)} = \rho_{g2}^{(s)} = 0$, which can be shown by solving the system of Eqs. (B4-B5) and using the fact that $\Gamma_{H_1} + \Gamma_{H_2} + \Gamma_{C_k} + \gamma_d > 0$. Furthermore, we introduce the variable $r = \rho_{gg}^{(s)} / (\rho_{gg}^{(s)} + \rho_{11}^{(s)})$ to obtain

$$\hat{\rho}_A = |g\rangle r \langle g| + |1\rangle (1-r) \langle 1|. \quad (\text{C6})$$

The system of equations using the projectors on these two groups is given by

$$\begin{aligned}\dot{p}_A &= 2(\Gamma_{C_2} + \gamma_{d_b})p_2 - 2((1-r)\gamma_{d_f} + r\Gamma_{H_2})p_A - iJ(\rho_{21} - \rho_{12}) \\ &\quad + 2(\gamma_{d_f} - \Gamma_{H_2})[(1-r)\rho_{gg} - r\rho_{11}],\end{aligned}\tag{C7}$$

$$\begin{aligned}\dot{p}_2 &= 2((1-r)\gamma_{d_f} + r\Gamma_{H_2})p_A - 2(\Gamma_{C_2} + \gamma_{d_b})p_2 - iJ(\rho_{12} - \rho_{21}) \\ &\quad - 2(\gamma_{d_f} - \Gamma_{H_2})[(1-r)\rho_{gg} - r\rho_{11}],\end{aligned}\tag{C8}$$

$$\begin{aligned}\langle g | \mathcal{Q}[\dot{\hat{\rho}}] | g \rangle &= riJ(\rho_{21} - \rho_{12}) + 2((1-r)(\Gamma_{C_1} + r\gamma_{d_f}) \\ &\quad - r(\Gamma_{H_1} + (1-r)\Gamma_{H_2}))p_A + 2((1-r)\Gamma_{C_2} - r\gamma_{d_b})p_2 \\ &\quad - 2(\Gamma_{H_1} + (1-r)\Gamma_{H_2} + \Gamma_{C_1} + r\gamma_{d_f})[(1-r)\rho_{gg} - r\rho_{11}],\end{aligned}\tag{C9}$$

$$\langle g | \mathcal{Q}[\dot{\hat{\rho}}] | 1 \rangle = \dot{\rho}_{g1},\tag{C10}$$

$$\langle g | \mathcal{Q}[\dot{\hat{\rho}}] | 2 \rangle = \dot{\rho}_{g2},\tag{C11}$$

$$\langle 1 | \mathcal{Q}[\dot{\hat{\rho}}] | 2 \rangle = \dot{\rho}_{12}.\tag{C12}$$

The other diagonal terms do not introduce more information since $\langle 1 | \mathcal{Q}\mathcal{L}[\hat{\rho}] | 1 \rangle = -\langle g | \mathcal{Q}\mathcal{L}[\hat{\rho}] | g \rangle$ and $\langle 2 | \mathcal{Q}\mathcal{L}[\hat{\rho}] | 2 \rangle = 0$, and other terms are deduced using Hermiticity of $\hat{\rho}$. To obtain an equation of p_A and p_2 only, we need to substitute $\rho_{12} - \rho_{21}$ and $(1-r)\rho_{gg} - r\rho_{11}$ in Eqs. (C7-C8). The first quantity is replaced using the same procedure as in previous subsection. Regarding the second quantity, we can isolate it by imposing steady state in Eq. (C9) $\langle g | \mathcal{Q}\mathcal{L}[\hat{\rho}] | g \rangle = 0$,

$$\frac{(1-r)\rho_{gg} - r\rho_{11} = ((1-r)(\Gamma_{C_1} + r(\beta + \gamma_{d_f})) - r(\Gamma_{H_1} + (1-r)\Gamma_{H_2}))p_A + ((1-r)\Gamma_{C_2} - r(\beta + \gamma_{d_b}))p_2}{r(\beta + \gamma_{d_f}) + \Gamma_{H_1} + (1-r)\Gamma_{H_2} + \Gamma_{C_1}}.\tag{C13}$$

Substituting this into Eqs. (C7-C8), we obtain the final set of kinetic equations for the two groups in the steady state

$$\dot{p}_A = -k_{2A}p_A + k_{A2}p_2,\tag{C14}$$

$$\dot{p}_2 = k_{2A}p_A - k_{A2}p_2,\tag{C15}$$

where the rates are given by Eqs. (29-30).

REFERENCES

¹J. J. J. Roden and K. B. Whaley, [Phys. Rev. E **93** \(2016\)](#).

- ²K.-D. Wu, A. Streltsov, B. Regula, G.-Y. Xiang, C.-F. Li, and G.-C. Guo, [Advanced Quantum Technologies](#) **4**, 2100040 (2021).
- ³F. Ghasemi and A. Shafiee, [Biosystems](#) **197**, 104209 (2020).
- ⁴S. R. Patil, H. Mohammad, V. Chawda, N. Sinha, R. K. Singh, J. Qi, and M. P. Anantram, [ACS Applied Nano Materials](#) **4**, 10029 (2021).
- ⁵M. Ottolenghi, in *Biomembranes Part I: Visual Pigments and Purple Membranes II* (Elsevier, 1982) pp. 470–491.
- ⁶A. Wand, I. Gdor, J. Zhu, M. Sheves, and S. Ruhman, [Annual Review of Physical Chemistry](#) **64**, 437 (2013).
- ⁷D. Polli, P. Altoè, O. Weingart, K. M. Spillane, C. Manzoni, D. Brida, G. Tomasello, G. Orlandi, P. Kukura, R. A. Mathies, M. Garavelli, and G. Cerullo, [Nature](#) **467**, 440 (2010).
- ⁸T. V. Tscherbul and P. Brumer, [J. Phys. Chem. A](#) **118**, 3100 (2014).
- ⁹S. Jin, R. C. Snoeberger, A. Issac, D. Stockwell, V. S. Batista, and T. Lian, [J. Phys. Chem. B](#) **114**, 14309 (2010).
- ¹⁰Z. Piontkowski and D. W. McCamant, [Journal of the American Chemical Society](#) **140**, 11046 (2018).
- ¹¹D. Segal, A. Nitzan, and P. Hänggi, [J. Chem. Phys.](#) **119**, 6840 (2003).
- ¹²N. Li, J. Ren, L. Wang, G. Zhang, P. Hänggi, and B. Li, [Reviews of Modern Physics](#) **84**, 1045 (2012).
- ¹³Z. Xu, [Theoretical and Applied Mechanics Letters](#) **6**, 113 (2016).
- ¹⁴M. Kilgour and D. Segal, [Phys. Rev. E](#) **98** (2018).
- ¹⁵D. Manzano, [PLoS ONE](#) **8**, e57041 (2013).
- ¹⁶R. de J. León-Montiel, I. Kassal, and J. P. Torres, [J. Phys. Chem. B](#) **118**, 10588 (2014).
- ¹⁷E. Zerah-Harush and Y. Dubi, [J. Phys. Chem. Letters](#) **9**, 1689 (2018).
- ¹⁸T. V. Tscherbul and P. Brumer, [J. Chem. Phys.](#) **148**, 124114 (2018).
- ¹⁹V. Janković and T. Mančal, [J. Chem. Phys.](#) **153**, 244110 (2020).
- ²⁰P.-Y. Yang and J. Cao, [J. Phys. Chem. Letters](#) **11**, 7204 (2020).
- ²¹K. A. Jung and P. Brumer, [J. Chem. Phys.](#) **153**, 114102 (2020).
- ²²M. Galperin, M. A. Ratner, and A. Nitzan, [Journal of Physics: Condensed Matter](#) **19**, 103201 (2007).
- ²³I. Novrotskaya and S. Hammes-Schiffer, [J. Chem. Phys.](#) **131**, 024112 (2009).

- ²⁴J. E. Subotnik, T. Hansen, M. A. Ratner, and A. Nitzan, *J. Chem. Phys.* **130**, 144105 (2009).
- ²⁵M. Zwolak, *J. Chem. Phys.* **153**, 224107 (2020).
- ²⁶K. Hoki and P. Brumer, *Procedia Chemistry* **3**, 122 (2011).
- ²⁷S. Axelrod and P. Brumer, *J. Chem. Phys.* **149**, 114104 (2018).
- ²⁸S. Axelrod and P. Brumer, *J. Chem. Phys.* **151**, 014104 (2019).
- ²⁹J. Cao and R. J. Silbey, *J. Phys. Chem. A* **113**, 13825 (2009).
- ³⁰J. Wu, F. Liu, J. Ma, R. J. Silbey, and J. Cao, *J. Chem. Phys.* **137**, 174111 (2012).
- ³¹J. Liu and D. Segal, *J. Phys. Chem. B* **123**, 6099 (2019).
- ³²P. J. M. Johnson, M. H. Farag, A. Halpin, T. Morizumi, V. I. Prokhorenko, J. Knoester, T. L. C. Jansen, O. P. Ernst, and R. J. D. Miller, *J. Phys. Chem. B* **121**, 4040 (2017).
- ³³P. Brumer, *J. Phys. Chem. Letters* **9**, 2946 (2018).
- ³⁴R. Zwanzig, *Physical Review* **124**, 983 (1961).
- ³⁵H. Mori, *Progress of Theoretical Physics* **33**, 423 (1965).
- ³⁶H. Feshbach, *Annals of Physics* **5**, 357 (1958).
- ³⁷H. Feshbach, *Annals of Physics* **19**, 287 (1962).
- ³⁸D. Manzano, *AIP Adv.* **10**, 025106 (2020).
- ³⁹H. J. Kreuzer, *Nonequilibrium thermodynamics and its statistical foundations* (Clarendon Press Oxford University Press, Oxford New York, 1981).
- ⁴⁰M. V. Fischetti, *Journal of Applied Physics* **83**, 270 (1998).
- ⁴¹G. A. Watson, ed., *Numerical Analysis* (Springer Berlin Heidelberg, 1976).
- ⁴²G. S. Agarwal, *Quantum Optics* (Cambridge University Press, 2013).
- ⁴³Z. Ficek and S. Swain, *Quantum Interference and Coherence: Theory and Experiments* (Springer, 2004).
- ⁴⁴M. Scully and M. S. Zubairy, *Quantum Optics* (Cambridge University Press, 1997).
- ⁴⁵T. V. Tscherbul and P. Brumer, *J. Chem. Phys.* **148**, 124114 (2018).
- ⁴⁶M. Thoss, H. Wang, and W. H. Miller, *J. Chem. Phys.* **115**, 2991 (2001).
- ⁴⁷D. Xu and J. Cao, *Frontiers of Physics* **11**, 110308 (2016).
- ⁴⁸G. S. Engel, T. R. Calhoun, E. L. Read, T.-K. Ahn, T. Mančal, Y.-C. Cheng, R. E. Blankenship, and G. R. Fleming, *Nature* **446**, 782 (2007).
- ⁴⁹C. Chuang and P. Brumer, *J. Chem. Phys.* **152**, 154101 (2020).
- ⁵⁰M. B. Plenio and S. F. Huelga, *New J. Phys.* **10**, 113019 (2008).

- ⁵¹P. Rebentrost, M. Mohseni, I. Kassal, S. Lloyd, and A. Aspuru-Guzik, *New J. Phys.* **11**, 033003 (2009).
- ⁵²S. Banerjee, *Open Quantum Systems: Dynamics of Classical Evolution* (Springer, 2018).
- ⁵³S. Hahn and G. Stock, *J. Phys. Chem. B* **104**, 1146 (2000).
- ⁵⁴A. Gonzalez, E. Kengmana, M. Fonseca, and G. Han, *Materials Today Advances* **6**, 100058 (2020).
- ⁵⁵T. Takagahara, E. Hanamura, and R. Kubo, *J. Phys. Soc. Jpn.* **44**, 728 (1978).
- ⁵⁶L. Joubert-Doriol and A. F. Izmaylov, *J. Chem. Phys.* **142**, 134107 (2015).
- ⁵⁷P. P. Hofer, M. Perarnau-Llobet, L. D. M. Miranda, G. Haack, R. Silva, J. B. Brask, and N. Brunner, *New J. Phys.* **19**, 123037 (2017).
- ⁵⁸S. Mukamel, *Principles of Nonlinear Optical Spectroscopy* (Oxford University Press, 1995).
- ⁵⁹M. Shapiro and P. Brumer, *Quantum Control of Molecular Processes* (Wiley-VCH Verlag GmbH & Co. KGaA, 2011).
- ⁶⁰X.-P. Jiang and P. Brumer, *J. Chem. Phys.* **94**, 5833 (1991).
- ⁶¹M. Yanagawa, K. Kojima, and T. Yamashita, et al., *Sci. Rep.* **5**, 11081 (2015).
- ⁶²T. Yamamoto, *J. Chem. Phys.* **33**, 281 (1960).
- ⁶³W. H. Miller, S. D. Schwartz, and J. W. Tromp, *J. Chem. Phys.* **79**, 4889 (1983).
- ⁶⁴T. Yamamoto, *J. Chem. Phys.* **33**, 281 (1960).
- ⁶⁵A. Redfield, in *Advances in Magnetic Resonance* (Elsevier, 1965) pp. 1–32.
- ⁶⁶D. Egorova, M. Thoss, W. Domcke, and H. Wang, *J. Chem. Phys.* **119**, 2761 (2003).
- ⁶⁷S. Hahn and G. Stock, *Chemical Physics* **259**, 297 (2000).